Contents lists available at ScienceDirect

Materials Today Communications

journal homepage: www.elsevier.com

Tribological and corrosion Behavior of Duplex Coated AISI 316L using plasma based ion implantation and deposItion

Laura S. Vaca [a, *], Juan P. Quintana [b, c], Daniel Vega [d], Adriana Márquez [b, c], Sonia P. Brühl [a]

[a] Surface Engineering Group, UTN-FRCU, Ing. Pereira 676, E3264BTD, Concepción del Uruguay, Argentina
[b] Universidad de Buenos Aires, Facultad de Ciencias Exactas y Naturales, Departamento de Física, Buenos Aires, Argentina
[c] Universidad de Buenos Aires, Consejo Nacional de Investigaciones Científicas y Técnicas, Instituto de Física del Plasma (INFIP), Facultad de Ciencias Exactas y Naturales, Ciudad Universitaria Pab. I, 1428, Buenos Aires, Argentina
[d] Physical Department of Condensed Matter (GIyA, CNEA), Av. Gral Paz 1499, B1650, San Martín, Buenos Aires, Argentina

ARTICLE INFO

Keywords:
Duplex process
Nitriding
Plasma based ion implantation and deposition
TiN
Wear
Corrosion

ABSTRACT

The implementation of a duplex process, which combines plasma nitriding with hard coatings obtained by cathodic arc, on stainless steel substrates has faced adhesion problems that affected the wear and corrosion behavior of the treated surfaces. One variation of the cathodic arc process, which could improve the adhesion, is its combination with plasma ion implantation.

This work presents results of the wear and corrosion behavior of duplex TiTiN bilayer coatings obtained by cathodic arc deposition combined with ion implantation (PBII&D) on plasma nitrided AISI 316 L stainless steel In order to compare the application of PBII&D in duplex processes against conventional cathodic arc deposition, other two types of samples were obtained; one group of samples was coated using the same experimental device with the substrate at floating potential and the other one with a commercial PVD system.

The coatings were characterized by SEM, XRD, and nanoindentation. The adhesion was evaluated by the Scratch Test and Rockwell C indentation. The wear resistance was analyzed by the pin-on-disk test and the corrosion behavior was evaluated by means of anodic polarization tests in NaCl solution, as well as by the Salt Spray Fog Test.

The PBII&D bilayer coatings showed better adhesion while the commercial PVD TiN coatings presented the smallest wear volume loss, but the delamination inside and around the track evidenced adhesion problems. Corrosion resistance was improved in all coatings benchmarked against nitride substrates, but PBII&D processes offered better protection.

1. Introduction

Austenitic stainless steels, like AISI 316 L, are usually used in aggressive industrial environments, such as food, petrol and chemical industries, due to the high Cr content which allows the formation of a thin oxide layer that protects them against corrosion. However, its low hardness and poor wear resistance make it necessary to improve the tribological properties by surface modification treatments with the purpose of extending the application range [1,2].

Several surface treatments and thin film deposition processes have been designed in order to improve hardness, wear and corrosion properties of these steels. Plasma nitriding is a useful thermochemical process for hardening stainless steels which increases the wear resistance, but the corrosion resistance could be affected if the nitrogen combined with the free chromium near the surface instead of remaining in solution [3,4]. Physical vapor deposition (PVD) TiN ceramic coatings are widely used for hardening cutting tools, extending wear life and, because of their chemical inertness and biocompatibility, are used as biomaterials or in mechanical components working in harsh industrial environments. Cathodic arc deposition is a very required PVD technique because the high ionization degree of the plasma with ion energy in the range of tens to a few hundred eV promotes the formation of adherent and dense coatings, which increases hardness and wear resistance [5,6]. Plasma Based Ion Implantation and Deposition (PBII&D) is an alternative method in which a high negative pulsed voltage is applied to the substrate, increasing the ion energy to the

* Corresponding author.
Email address: vacal@frcu.utn.edu.ar (L.S. Vaca)

https://doi.org/10.1016/j.mtcomm.2020.101892
Received 23 June 2020; Received in revised form 12 November 2020; Accepted 13 November 2020
Available online xxx
2352-4928/

Table 1
Main deposition parameters.

Condition	Bias [kV]	Pressure [Pa]	Gases	Arc Current [A]	Cathodes Number	Distance sample-target [m]	Time Ti/TiN [s]	Temperature [°C]	Interlayer
TiTiN + I	− 6	3×10^{-2}	N_2	100	1	0.25	120/1020	300	Ti
TiTiN	floating	3×10^{-2}	N_2	100	1	0.25	120/1020	300	Ti
TiNS	− 0.250	2	N_2	60	4	0.25	1200	350	none

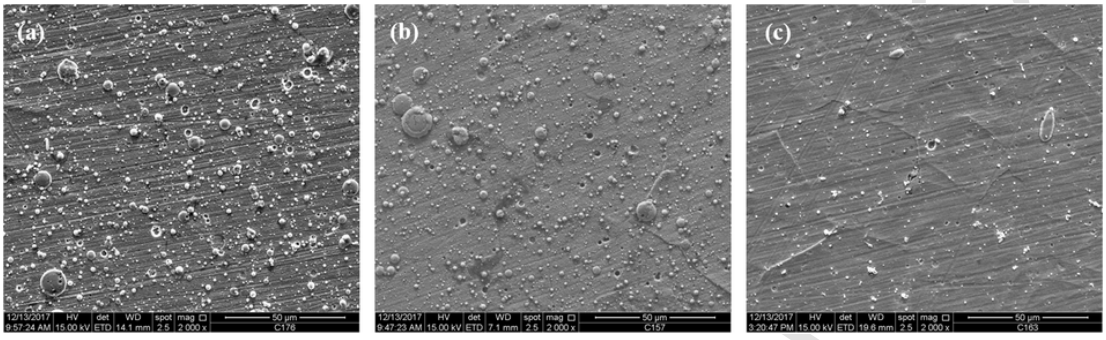

Fig. 1. SEM surface micrographs 2000x: (a) TiTiN + I, (b) TiTiN, (c) TiNS.

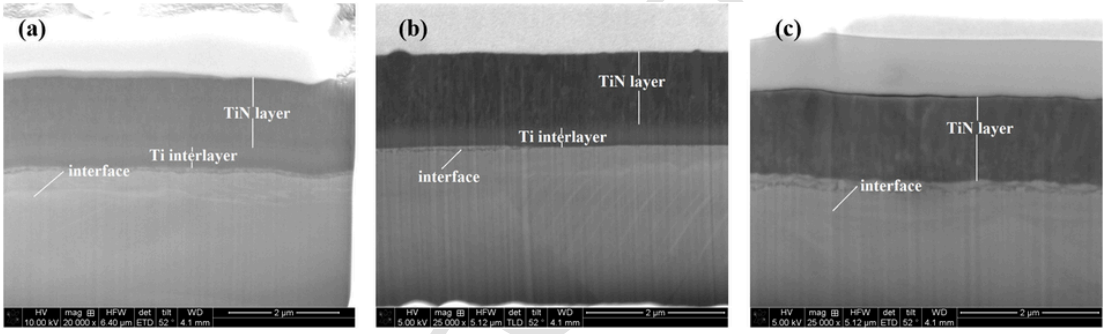

Fig. 2. FIB-SEM images layer, interlayer and interface thickness: (a) TiTiN + I, (b) TiTiN, (c) TiNS.

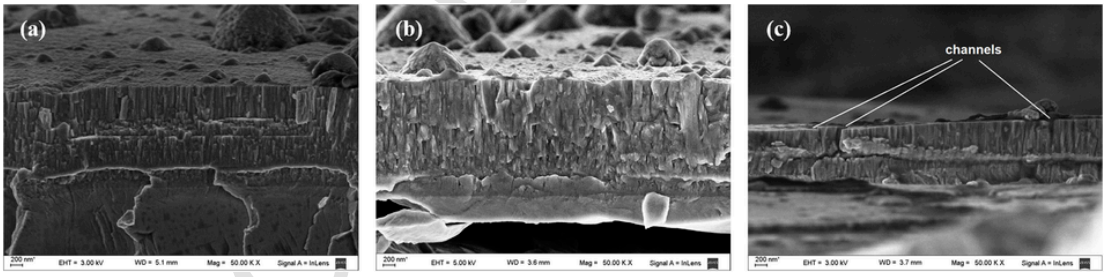

Fig. 3. SEM images columnar structure: (a) TiTiN + I, (b) TiTiN, (c) TiNS.

Table 2
Roughness values and mechanical properties of the different layers.

Sample	Ra (μm)	H (GPa)	E (GPa)	H/E	H^3/E^2
TiTiN + I	0.18 ± 0.03	25.4 ± 0.7	310 ± 5	0.084 ± 0.004	0.171 ± 0.007
TiTiN	0.14 ± 0.02	26 ± 1	358 ± 10	0.074 ± 0.005	0.134 ± 0.009
TiNS	0.08 ± 0.01	32.4 ± 0.8	354 ± 5	0.094 ± 0.004	0.271 ± 0.010
Nitrided	0.09 ± 0.01	13.0 ± 0.2	144 ± 3	0.090 ± 0.003	0.105 ± 0.004
Blank	0.08 ± 0.01	2.45 ± 0.05	190 ± 2	0.013 ± 0.001	0.0040 ± 0.0003

range of keV. These energetic ions impinge at the surface and they are implanted in it during the pulse meanwhile the relative low energy ions are deposited at the surface between pulses. The ions penetrate a few atomic layers creating a diffuse interface from the beginning of the coating deposition process, which increases the adhesion and densifies the film while it is growing, thus avoiding the formation of channels or pores [5–10]. Duplex treatments, nitriding + coating, allow to achieve properties that would be difficult to obtain with a single technique. In the case of combining plasma nitriding and PVD hard coatings on tool steels, it has been reported that the nitrided layer provides a mechanical support to the film that improves the wear resistance [11–13].

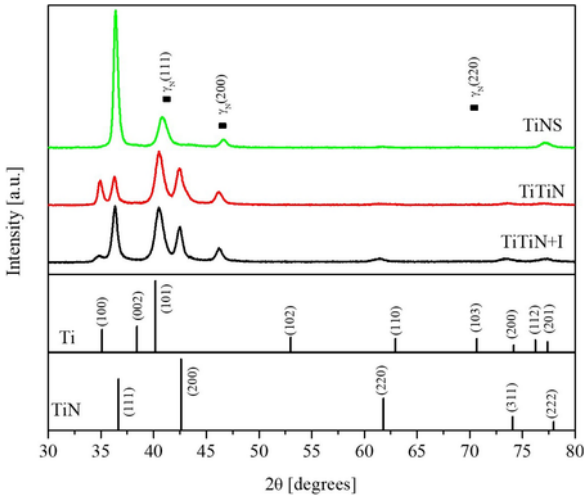

Fig. 4. XRD patterns in Bragg-Brentano geometry.

Table 3
Structural parameters of TiN coatings.

Samples	Microstress 10^{-3}[no unit]	Crystallite size [nm]	Residual stress [GPa]
TiTiN + I	7.9 ± 3.0	17 ± 2	−5.10 ± 0.91
TiTiN	6.7 ± 1.9	21 ± 3	−5.03 ± 0.45
TiNS	6.3 ± 0.7	21 ± 1	−6.69 ± 0.42

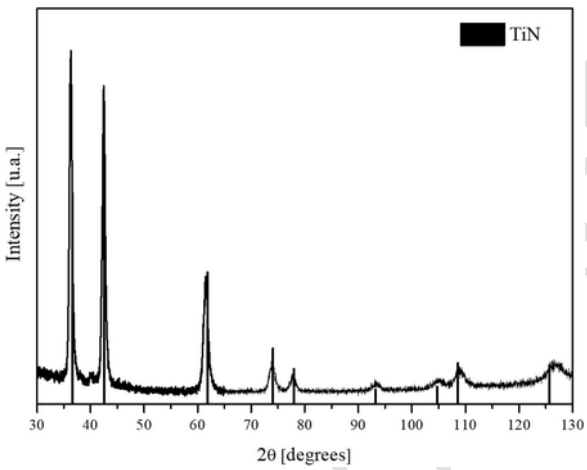

Fig. 5. XRD pattern in grazing incidence geometry with incidence angle α = 1°.

Coating adhesion has a crucial influence both on wear and corrosion behavior; in a previous work the authors demonstrated that an effective pre-treatment of a nitrided substrate before coating it and the

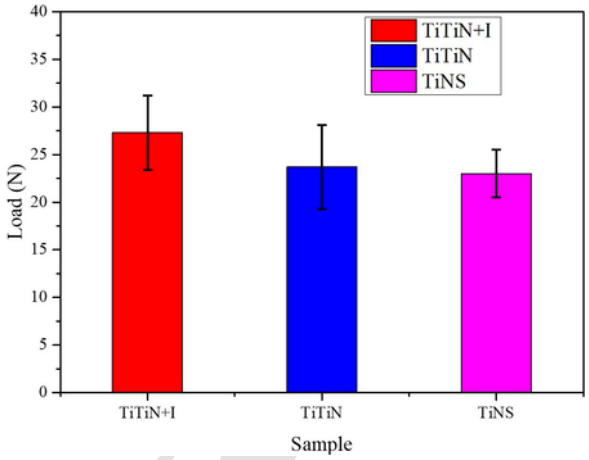

Fig. 6. Scratch test critical load TiTiN + I, TiTiN and TiNS, mean values and errors.

introduction of a thin Ti interlayer are essential to achieve good adhesion [14]. The tribological properties of the films are also improved by the presence of compressive residual stresses, which helps to reduce the crack propagation too [7,15,16].

Several authors have studied mechanical, wear and corrosion performance of different PVD hard coatings obtained by magnetron sputtering, ion plating, cathodic arc, or PBII&D. The study of structure and microhardness of TiN coatings deposited using magnetron sputtering on pre-nitrided AISI 304 steel showed a significant increase of microhardness of duplex treated samples respect to the nitride one [17]. Microstructure and tribological behavior of TiN coatings deposited with CAD on nitride AISI 316 L were investigated by Las Heras et. Al [18]. This research showed that the duplex treatment improved significantly the wear resistance of the surfaces during sliding/ contact tests respect to the substrates only nitrided. Some of the authors of the present work carried out the characterization of TiN coatings deposited with CAD and PBII&D on pre-nitrided AIS I316 L [19]. The work focused on the microstructure and the corrosion behavior found the best corrosion behavior for the PBII&D coatings. However, TiN coatings grown with PBII&D over plasma nitrided austenitic stainless steel have not yet been extensively studied from the mechanical point of view.

In this work, wear and corrosion behavior of Ti/TiN bilayer coatings obtained by PBII&D over a plasma nitrided AISI 316 L stainless steel were evaluated and compared with cathodic arc PVD Ti/TiN, without polarization and a PVD commercial TiN coatings. Results of wear and corrosion tests were related to mechanical structure and adhesion characteristics of the coatings.

2. Material and methods

Cylindrical 5 mm high disks were cut from a 25 mm in diameter AISI 316 L bar. The face to be nitrided was grinded with SiC paper up to #1000 grid. The direct current plasma nitriding (DCPN) process was carried out into an industrial equipment of IONAR S.A (Argentina) for

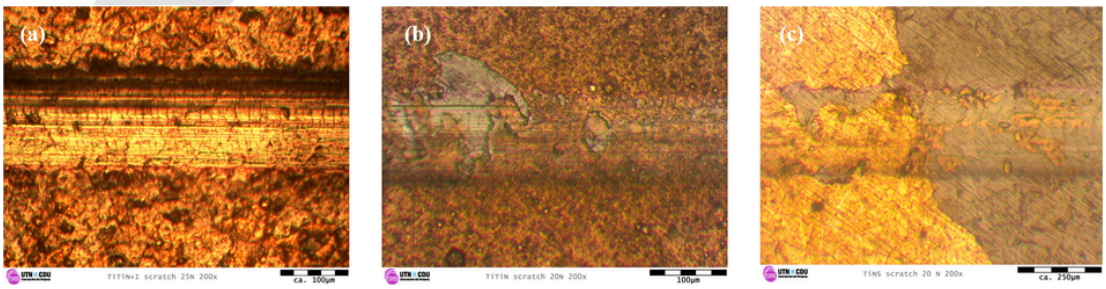

Fig. 7. Scratch test 200x: (a) 25 N for TiTiN + I, (b) 20 N for TiTiN, (c) 20 N for TiNS.

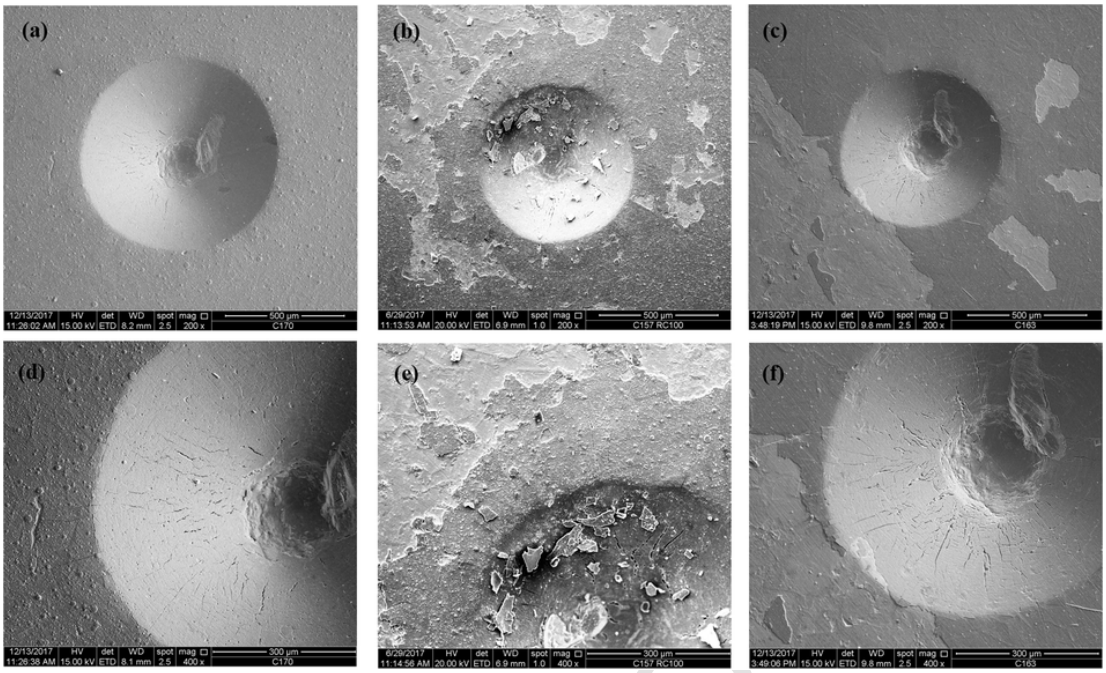

Fig. 8. SEM images RC Indentation: (a) TiTiN + I 200x, (b) TiTiN 200x, (c) TiNS 200x, (d) TiTiN + I 400x, (e) TiTiN 400x, (f) TiNS 400x.

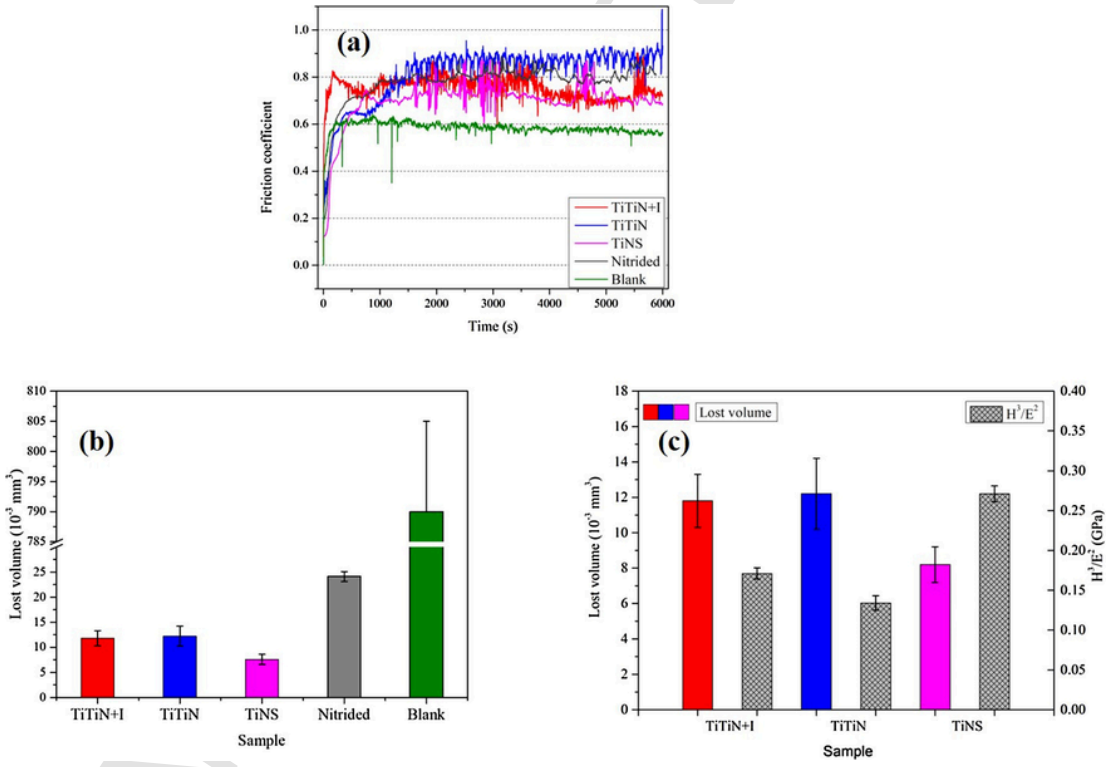

Fig. 9. Pin-on-disk TiTiN + I, TiTiN, TiNS, graphs: (a) friction coefficient, (b) lost volume (c) lost volume and H^3/E^2 ratio.

20 h, at 420 °C, in a gas mixture of 20 % N_2 + 80 % H_2. The nitrided samples were grinded again with #1000 grid for 1 min with a small load without significantly affecting the nitride layer. The nitrided samples were divided into four groups. Two groups called TiTiN and TiTiN + I were coated with Ti/TiN bilayers in an experimental cathodic arc device. A third group denominated TiNS was coated with TiN monolayers into an industrial device of SUDOSILO S.A (Argentina). A fourth group was not coated to be used as a benchmark (Nitrided) and, for the same reason, a fifth group of nude steel samples (Blank) was considered.

The experimental cathodic arc device has been described in a previous work [14]. The arc current was set at 100 A. The substrates were located approximately 0.25 m away from the cathode, keeping the temperature at 300 °C. TiTiN samples were insulated from the device biasing at floating potential and TiTiN + I samples were biased with negative pulses (6 kV, 50μs width, at 200 Hz). The nitrided substrates of

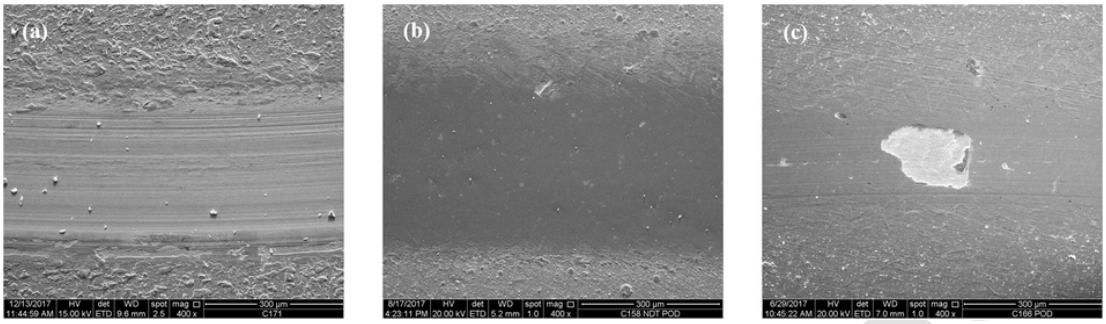

Fig. 10. Micrograph of the Pin-on-disk wear track: (a) TiTiN + I, (b) TiTiN, (c) TiNS.

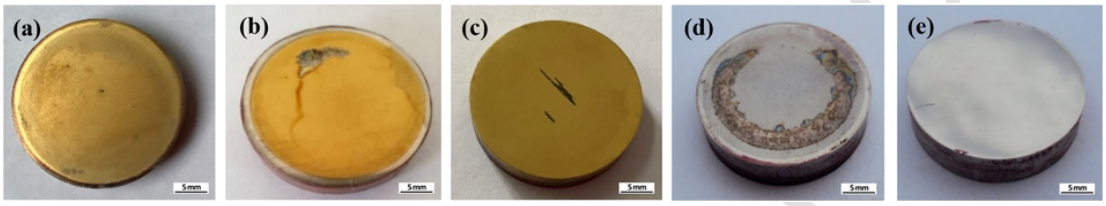

Fig. 11. Surface photos after the salt fog spray test: (a) TiTiN + I, (b) TiTiN, (c) TiNS, (d) Nitrided, (e) Blank.

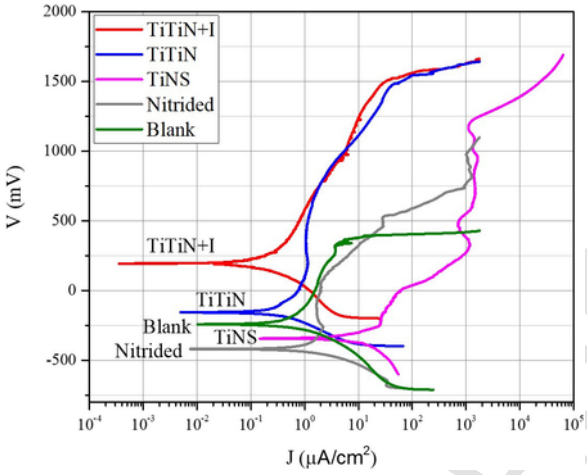

Fig. 12. Polarization curves of TiTiN + I, TiTiN, TiNS, Nitrided and Blank samples.

Table 4
Anodic – cathodic polarization quantitative data.

Sample	E_{corr} mV vs SCE	J_{300mV} μA/cm²	E_{bk} mV vs SCE
TiTiN + I	203 ± 2	0.31 ± 0.08	1524 ± 9
TiTiN	−153 ± 4	1.04 ± 0.04	1496 ± 8
TiNS	−340 ± 4	1095 ± 22	42 ± 3
Nitrided	−419 ± 5	9.62 ± 0.11	542 ± 6
Blank	−240 ± 2	3.68 ± 0.15	340 ± 8

TiTiN + I and TiTiN samples were chemically cleaned and sputtered with an Ar-H_2 (50 %-50 %) glow discharge following the optimized protocol described in Ref. 14. The Ti layer was deposited with a discharge of 2 min duration at a pressure lower than 10^{-2} Pa. The TiN coating was obtained introducing a nitrogen flow at a 3×10^{-2} Pa working pressure, exposing the sample to the discharge for 17 min.

The commercial device had four evaporators at different heights and the samples were placed on horizontal platforms with satellite movement that maintained an average distance to the cathode of (0.25 + 0.07) m. The substrates were heated at 350 °C and biased at –250 V DC, and the arc current set at 60 A. Pre-treatment of TiNS samples consisted of sputtering with Ti ions. The ion bombardment was carried out in vacuum arc discharge increasing the bias of the samples to –700 V with the purpose of making the bombardment predominant, thus avoiding Ti deposition. The TiN films were deposited in a N_2 atmosphere at a working pressure of 2 Pa, exposing the sample to the discharge for 20 min.

The main parameters of three conditions are summarized in Table 1.

Crystalline structure and residual stresses in the different films were analyzed with X-ray diffraction (XRD). Diffraction patterns were measured in Bragg Brentano and grazing incidence geometries using a PHILIPS PW1710 and a Panalytical Empyrean diffractometer, respectively. In both devices, the Cu Kα radiation was employed, with an average wavelength of λ = 1.5418 Å. Bragg Brentano patterns were measured in 2θ ranges 30° - 80° and 100° - 130° with a step size of 0.03°. In grazing incidence geometry, the incidence angle (α) was set at 1º and 2θ varied in the range 30° - 130° with a step size of 0.02°. The TiN crystallite size was calculated with the Scherrer´s formula from the (111) peak broadening, subtracting the instrumental peak broadening (β). The microstress was estimated by applying the Williamson-Hall method [20]. This technique allows the calculation of the microstress from the slope when plotting $\beta.\cos(\theta) vs. sin(\theta)$. Both film morphology and thickness were analyzed by Optical Microscopy (OM) and Scanning Electron Microscopy (SEM), combined with Focused Ion Beam, FE-SEM/FIB Helios Nanolab 600 (FEI company), to analyse the cross section after ion milling with gallium atoms.

The coating roughness values were obtained by scanning with a Laser Confocal Scanning Microscope OLYMPUS OLS4100, in a representative square area of 7 × 7 μm². The obtained images were analyzed with the microscope software LEXT® and the average roughness was estimated from the average and the standard deviation of 10 measurements in each sample.

The nanoindentation tests were performed according to ISO 14577–1, in a Triboindenter Hysitron equipped with a Berkovich indenter, using a 10 mN load and 2 s of indentation time. Each sample was tested in six different and distant positions and in each one, a grid of 4 × 4 indentations were performed, 10 μm away from each other. The penetration was lower than 110 nm in all cases and the total number of indentations for each sample was 96. Not only Hardness (H) and Young Modulus (E) of the films were measured, but also the elastic strain to failure (H/E) and (H3/E2) ratios were calculated in order to correlate them with the tribological behavior [21–23].

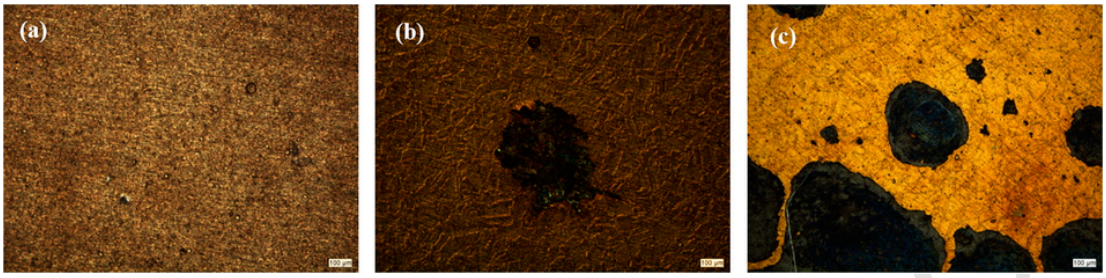

Fig. 13. Optical Micrographs of corrosion pits after the polarization test: (a) TiTiN + I, (b) TiTiN, (c) TiNS.

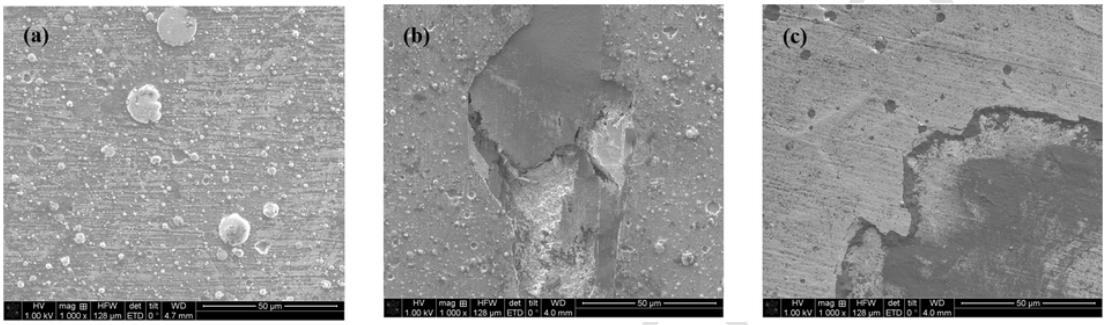

Fig. 14. SEM pictures of the corroded region analyzed by EDS (a) TiTiN + I, (b) TiTiN, (c) TiNS.

Table 5
EDS quantitative data in the pits of selected samples.

Sample	N At%	Fe At%	Cr At%	Ti At%
TiTiN + I	3.63 ± 0.18	–	–	33.42 ± 1.70
TiTiN	10.79 ± 0.54	48.72 ± 2.40	17.93 ± 0.90	–
TiNS	3.29 ± 0.16	28.74 ± 1.40	20.77 ± 1.04	0.16 ± 0.01

The coating adhesion was evaluated by the Scratch Test with constant load and Rockwell C indentation. The scratch experiments were carried out with a Scratch Tester designed and built according to ASTM C-1624 standard [24], under unlubricated conditions and at room temperature (~20 °C). The speed of the indenter was 10 mm/min forward, the load was varied from 5 N to 40 N in steps of 5 N. Scratch scars images were obtained with an optical microscope (OM) and a scanning electron microscope (SEM). The criterion considered to classify the damage was with a single level (L_{C1}), where the critical load corresponds to the value where the first failure occurs in the film [24]. The Rockwell C indentation test was realized with a conical diamond indenter, and the imprints were observed with OM and SEM to classify them as acceptable or not, according to the VDI 3198 Standard [25].

Wear resistance was studied in a pin-on-disk test, with a machine designed and built according to the ASTM G99 – 95a Standard [26]. The tests were carried out at room temperature with a relative humidity of about 60 %, with a 3 N load at sliding speed of 0.10 ms^{-1}, 500 m sliding distance, and an alumina ball (Al_2O_3 Ø 6 mm) as the counterpart. The wear track profiles were measured with a mechanical profilometer and White Light Interferometry (WLI). The lost volumes were calculated using geometric considerations.

The corrosion resistance was evaluated by Salt Spray Fog and Potentiodynamic Polarization Tests. The former test was conducted for 100 h in sodium chloride solution, at 35 °C temperature reproducing a corrosive environment, following the ASTM International B117 – 03 Standard [27]. When the samples were removed from the chamber, the surfaces were washed with water and dried with tissue paper, before taking a photograph. The Potentiodynamic Polarization test was carried out in an electrolytic solution of sodium chloride at 3.5 % p/p at room temperature using a potentiostat Teq_04, connected to a conventional three-electrode system, with a saturated calomel electrode (SCE) as the reference electrode, a platinum wire as the counter electrode and the sample acted as the working electrode. The scan rate was 1 mV/s and 0.28 cm^2 was the effective work area, delimited with an o'ring. The corrosion potentials (E_{corr}) were determined in an open circuit potential configuration and the polarization curves, potential vs. current density were plotted afterwards. Images of corrosion pits were obtained by OM and SEM and analyzed by Energy Dispersive Spectroscopy (EDS). The corrosion tests were realized on three samples of each type.

Wear and corrosion tests were also applied to the nitrided samples without coating and to the nude steel or blank to be used as benchmarks.

3. Results and discussion

After plasma nitriding process, the average value of the Vickers microhardness at the nitrided surface, obtained from microhardness tests with a load of 4903 mN, was (1070 ± 70) $HV_{0,05}$. The thickness of the modified layer, measured on a cross-section with an optical microscope, was (104 ± 0,7) μm. Both the microhardness and the thickness measurements were similar to the results obtained in a previous work [14] and the procedure was the same as followed by other authors [18,19]. Due to the low load and short time employed for grinding before the coating process, the grinded samples did not show significant differences in hardness and thickness respect to the values reported above.

3.1. Coatings structure

The SEM examination of the coatings after the deposition process showed the presence of macroparticles, which are characteristic of cathodic arc PVD systems (Fig. 1). It is possible to observe that the TiTiN + I (Fig.1 (a)) and TiTiN (Fig. 1 (b)) surfaces did not show major differences between them. However, on the surface of TiNS (Fig. 1 (c)) the number and size of macroparticles were smaller than in the other samples. The work pressure, which is two orders of magnitude lower in the two first cases, could be the reason for the surface finishing differences. At a higher pressure, the nitride formation rate on the cathode

surface becomes bigger, increasing its melting point and therefore changing the macroparticle generation [28].

As it can be seen from the cross-section FIB – SEM micrographs presented in Fig. 2, the thickness of the TiN layer was about 1.5 μm for all the coatings and the thickness of Ti interlayer was around 0.5 μm for the TiTiN + I and TiTiN samples. Since the deposition times for the two types of bilayer coatings were the same, this similarity between the coating thicknesses indicate that the substrate bias conditions had not significant influence on the deposition rates.

Fig. 3 shows the SEM pictures obtained from the cross section of the samples after cryogenic fracture. A columnar structure and the compactness of the films, which are characteristics of this kind of treatment, can be clearly noted. The columnar width was (100 ± 10) nm for TiTiN and TiNS samples, and (50 ± 6) nm for TiTiN + I samples. The narrowing of TiTiN + I columns was probably induced by the higher kinetic energy acquired by the ions when the bias pulse was on. The structure zone diagram extended to the deposition of energetic ions and a large flux describes the structure features as a function of a generalized temperature and a normalized energy of particles that arrive on the surface, the different structure zones are delimited by approximately diagonal lines [29,30]. Therefore, at a similar process temperature, a higher energy of the impinged ions leads to the growth of narrower column grains. The structure of TiNS coatings presented some channels between columns, which can be observed in Fig. 3 (c).

The mean values of several average roughness measurements (Ra) for each coating group are shown in Table 2. TiNS samples presented a roughness similar to the substrates while TiTiN and TiTiN + I increased considerably, which could be attributed to a higher number of macroparticles on the surfaces. The hardness (H) and elastic modulus (E) obtained from nanoindentation measurements are also listed in Table 2. H/E and H^3/E^2 ratios were calculated and added to Table 2. H/E ratio is related to the plasticity index, which is proportional to the partitioning between the plastic work and the total (plastic plus elastic) work performed during indentation. A higher H/E ratio corresponds to a lower plasticity index and a more elastic contact. H^3/E^2 ratio is proportional to the load needed to initiate plastic deformation; this means that it is a measure of the resistance to plastic deformation [31,32]. As it can be observed in Table 2, the hardness of the coatings exceeded the hardness of the nitrided layer, and this in turn was much higher than that of the blank. These results agree that duplex treatments promote a smoother hardness gradient between the substrate and the film. TiNS coatings presented the higher H, H/E and H^3/E^2 values, indicating higher film resistance to plastic deformation, which some authors correlated with higher resistance to cracking [33].

Fig. 4 shows typical Bragg Brentano diffractograms in the 2θ range 30° - 80° for the three types of samples. Several peaks associated with expanded austenite (γ_N) from the nitrided substrate can be identified in all the samples. In TiTiN + I and TiTiN patterns, the peak associated with the Ti (100) plane (ICCD N°:00–044-1294) and all peaks of TiN (ICCD Nº:00–038-1420) can be identified. For TiNS samples, the diffractogram only exhibited the (111) and (222) TiN peaks, which indicated a preferential (111) orientation. From the broadening of TiN peaks, microstresses and crystallite size were estimated; the obtained values are reported in Table 3. For all coatings, crystallite size and microstress were around 20 nm and 7×10^{-3}, respectively.

Fig. 5 shows a grazing incidence diffractogram obtained from a TiTiN + I sample, where only peaks corresponding to TiN were observed. All the samples exhibited similar grazing incidence diffractograms as the one in Fig. 5. TiN residual stress was determined from the measurement of the diffraction peak position in grazing incidence patterns using the method of multiple *hkl* reflections [34]. The elastic strain (ε) of a *hkl* plane can be defined as:

$$\varepsilon = \frac{d - d_0}{d_0} \quad (1)$$

where d is the interplanar distance for the plane *hkl* associated with the position $2\theta_{hkl}$, d_0 is the interplanar distance for the plane *hkl* according to lattice parameter reported in the TiN reference card. Assuming TiN films as isotropic medium with rotationally symmetric biaxial stress state, ε can be related to $sin^2(\psi)$, being ψ the tilt angle, described as follows

$$\varepsilon = \frac{1+\nu}{E}\sigma\, sin^2(\psi) - \frac{2\nu}{E} \quad (2)$$

where ψ is calculated as the difference between Bragg angle and incidence angle ($\psi = \theta - \alpha$), σ is the residual stress, and $\nu = 0.25$ the TiN Poisson´s ratio [34]. The σ value was obtained from the slope of the linear fitting of ε vs $sin^2(\psi)$.

The results of residual stresses are summarized in Table 3. All samples presented compressive residual stress, characteristic of films grown by cathodic arc deposition, and TiNS attained the highest residual stress, around −6.7 GPa.

3.2. Adhesion

The bar graph of Fig. 6 presents the averages of critical loads L_C and the corresponding uncertainties obtained as the standard error determined from three Scratch Tests on ten samples for each condition.

No significant differences were found among L_C values obtained for each condition. However, the appearance of the tracks at the failure point were completely different. The typical damage suffered by the coatings on the tracks of the scratch test for each condition are shown in the optical micrographs of Fig. 7. Identifying the type of failure according to Bull´s table [24], TiTiN + I samples (Fig. 7(a)) showed arc tensile cracks, which is a series of semicircular micro cracks with no chipping TiTiN samples (Fig. 7(b)) exhibited recovery spallation, which is a small delamination inside and on the sides of the track; and the failure in all TiNS samples (Fig. 7(c)) was identified as "gross spallation". The latter corresponded to a big failure, where the delamination covered a large area around the track. This behavior has not been observed in any of the tests carried out on TiTiN and the TiTiN + I samples. The interface given by the Ti interlayer in both TiTiN + I and TiTiN coatings, unlike the TiNS samples, could be responsible for preventing the cracking propagation [14]

Rockwell C Indentation tests were also performed on the same samples. The results can be summarized as follows: all TiTiN + I samples, none of the TiTiN and only 10 % of the TiNS samples qualified as acceptable according to the VDI 3198 Standard [25]. This means that only the bilayer films grown with implantation presented a very good adhesion in this test. In Fig. 8, SEM pictures of the imprints are presented. Large zones of delamination were observed in both TiTiN and TiNS around the imprints. This implies a poor interfacial adhesion in which the main difference with the TiTiN + I samples is the implantation process, from where it can be inferred that the energy delivery by the ions in the first atomic layers could generate a graded interface between the substrate and the film, as other authors pointed out [7].

3.3. Wear and friction behavior

The results obtained from the pin-on-disk tests are shown in Fig. 9. The friction coefficients (CoF) registered along the total sliding distance are very irregular, even in the stationary stage. TiN unfiltered cathodic arc coatings generally do not improve the coefficient of friction, because macroparticles detach from the surface and can become trapped into the track acting as a third body and contributing to the formation of asperities or debris [35,36]. However, in the case of the TiNS

group, the mean stationary value of CoF is slightly lower than for the other two cases. This could be due to the smaller value of roughness and lower number of macroparticles. It is important to state that in all cases the ball was in contact with the coating during the whole test, since the wear track depth did not exceeded the film thickness, as

it was confirmed in the track profile measurement and SEM observation of the wear scars.

The volume losses for the samples of each condition are presented in the graph of Fig. 9(b), where the bars represent the mean value obtained from ten tests. It can be seen that all the coatings considerably improved the wear resistance compared to the nitrided sample, whose lost volume was already less than thirty times the lost volume of the bare steel. It was observed that the lost volume of the TiNS samples was lower than the lost volume of the TiTiN + I and TiTiN samples. In Fig. 9(c) lost volumes and H^3/E^2 ratios were plotted together in order to compare the behavior of both magnitudes more easily. The highest H/E and H^3/E^2 ratios of the TiNS coating indicate a higher elasticity and a higher resistance to plastic deformation, which contributed to a lower lost volume [37].

Representative SEM micrographs of pin-on-disk wear scars for each condition are presented in Fig. 10. Both the TiTiN + I and TiTiN bilayer samples showed only abrasion as the predominant mechanism, without any spallation. Nevertheless, in the TiNS monolayer spalling occurred and the substrate was visible, as it can be observed in Fig. 10(c). Since the characteristic dimensions of the holes are greater than 150 μm, the wear can be classified as severe. This result implies that if this type of damage occurs in a machine component, the machine must be taken out of service [38]. Some asperities and small wear debris formed during sliding can be observed in the worn tracks (Fig. 10(a)), their presence could contribute to an abrasion effect on wear [39–41]. The fact that the lost volume, the depth and the width of the tracks for TiTiN + I and TiTiN samples were slightly higher than for the TiNS ones agrees with the lower value of H^3/E^2 found for the bilayer coatings, which corresponds to a lower elasticity. Although some authors have associated a higher H^3/E^2 ratio with a higher resistance to cracking and therefore a high fracture toughness [37], Beake et al. figured out that this can be detrimental at high dynamic contacts [42]. They assessed that under highly loaded mechanical contact, effective durability and damage tolerance require resistance both to formation and propagation of cracks. Lower H/E and H^3/E^2 ratios imply a higher plasticity of the film allowing dissipative mechanisms to occur, such as plastic deformation, which helps to relieve the accumulated strain in the dynamic contact. Furthermore, it is well known that compressive residual stresses improve the tribological behavior, but high compressive stress may result in cohesion failures when the coating includes pores or pinholes, as the TiNS does in this case [38].

3.4. Corrosion

Fig. 11 shows typical images of the sample surfaces after the salt spray fog test. The TiTiN + I sample (Fig. 11(a)) did not present any corrosion signal in all the tests, neither pit, nor general corrosion, showing excellent corrosion resistance like the blank sample (Fig. 11(e)). It worth noting that the other coatings were slightly affected after the test, only a small delamination zone was registered on the TiTiN sample (Fig. 11(b)) and on the TiNS (Fig. 11(c)). The nitrided sample (Fig. 11(d)) exhibited an annular corrosion zone, indicating that this condition is not recommended for a saline environment.

Fig. 12 presents the polarization curves and it is evident that the bilayer coatings turned out to be much better corrosion resistant than the TiNS. The nitrided and the untreated samples present higher corrosion potentials and lower current densities for the same potential. Besides, the corrosion potential was positive only for TiTiN + I sample. The corrosion potential (E_{corr}), the current density value at 300 mV (J_{300mV}) and the breakdown potential (E_{bk}) for all the samples are listed in Table 4.

Although all samples presented a passive behavior, the zone of passive currents occurs at a different order of magnitudes of current densities and the amplitude of this zone is diffuse. It can be noted that nitriding slightly impairs the response to corrosion. It is remarkable that for the TiTiN + I and the TiTiN samples the breakdown potentials were much higher than for the TiNS samples and even comparing with the nitrided and the blank ones, as it can be seen in the curves of Fig. 12 and from the data in Table 4. This fact indicates a more extensive passive zone for bilayer coatings. The failure of the TiNS coatings in the corrosion protection could be caused by the structure defects, which probably contribute to generate channels (see Fig. 3(c)), through which the corrosive fluids reach the substrate. Meanwhile, in samples TiTiN + I and TiTiN, not only was the appearance of channels between the columns not detected, but the intermediate layer of Ti could have acted as a barrier preventing microcavities [43]. Similar results, where Ti/TiN bilayers presented better corrosion behavior than TiN coatings, have been previously published [44–46].

The OM images of Fig. 13 were obtained on the tested zone after the polarization test. In the TiTiN + I sample it was not possible to identify any pit, probably due to the fact that they were the same size as the depressions left by the detachment of some macroparticles, and the TiTiN sample presented some small pits and only a big one, of about 400 μm in diameter. Meanwhile, in the TiNS sample not only several pits of 200 μm and 400 μm were found, but also areas with film detachment, indicating a severe corrosion attack. In this case, when the electrolyte reached the substrate through some pit, crevice corrosion was promoted along the interface, consequently causing film delamination [47].

The SEM micrographs of the EDS tested surfaces for each condition are presented in Fig. 14, and the atomic percentages of more representative elements obtained from the analysis are listed in Table 5. The very low percentage of Ti and the high percentage of iron found on the pits, added to the change of color of the pit surface observed in Fig. 13, indicated that TiTiN and TiNS films were almost completely removed during the test and the substrate was exposed. Only the TiTiN + I film showed good integrity because after the test no signs of corrosion products or substrate components were detected.

4. Conclusions

- The bilayer TiTiN + I coatings presented the greatest refinement and compactness in the columnar structure. High compressive residual stresses were observed in all coatings, regardless of the deposition conditions. The adhesion tests showed that the TiTiN + I coatings had the best performance.
- The better performance of the TiNS monolayer in terms of lost volume can be attributed to a higher H^3/E^2 ratio associated with a higher elasticity of the films. However, the bilayer samples, which had the lowest H^3/E^2 values, had the advantage of withstanding greater plastic deformation by preventing detachment and peeling of the coating. The Ti interlayer would also have a positive effect in inhibiting crack propagation.
- Regarding the corrosion experiments, bilayer coatings improved the corrosion resistance, even in benchmarking against bare stainless steel. Analyzing the tested surface, only in the case of TiTiN + I, no signs of delamination were detected.

To sum up, TiTiN + I coatings obtained by PBII&D proved to be more compact and well attached; and the good adhesion and structure not only improved the wear behavior considerably, but also had a positive influence on the corrosion behavior. These results position the Ti/TiN coatings deposited with PBII&D combined with previous nitriding as a promising option to treat stainless steel components that must work under conditions similar to those presented in this study.

Uncited references

[43].

Declaration of Competing Interest

The authors declare that they have no known competing financial interests or personal relationships that could have appeared to influence the work reported in this paper.

Acknowledgments

The authors would like to thank the financial support of UTN PID MAUTICU 4716 TC, of UTN PID MAUTICU 5108 TC, of CONICET PIP 11220120100468, of University of Buenos Aires PID 20020150100103BA, of ANPCYT PID-2017-0001and CREATe-Network H2020-MSCA-RISE-2014 to enable researcher mobility.

The authors also gratefully acknowledge to Pablo Cirimello and Y-TEC (Argentina) for the XRD analysis, to Soledad Pereda and INTI (Argentina) for the SEM images and to Katherine Aristizabal and the Saarland University (Germany) for the FIB-SEM images.

References

[1] A.J. Sendriks, Corrosion of Stainless Steels, Corrosion Monograph Series Sponsored by the Electromechanical Society, second edition, A Wiley-Interscience Publication John Wiley & Sons, Inc, 1996.
[2] ASM Handbook Vol. 5. Surface Engineering, ASM Int., 1994.
[3] D. Manova, S. Mändl, Surface nitriding with energetic ions using plasma based ion implantation, in: Ronghua Wei (Ed.), Plasma Surface Engineering Research and Its Practical Applications, Research Signpost from Trivandrum, 2008, pp. 293–312.
[4] L. Gil, S. Brühl, L. Jiménez, O. León, R. Guevara, M.H. Staia, Corrosion performance of the plasma nitrided 316L stainless steel, Surf. Coat. Technol. 201 (2006) 4424–4429, https://doi.org/10.1016/j.surfcoat.2006.08.081.
[5] D.M. Sanders, A. Anders, Review of cathodic arc deposition technology at the start of the new millennium, Surf. Coat. Technol. 133–134 (2000) 78–90, https://doi.org/10.1016/S0257-8972(00)00879-3.
[6] Golnaz Taghavi Pourian Azar, Cagatay Yelkarasi, Mustafa Ürgen, The role of droplets on the cavitation erosion damage of TiN coatings produced with cathodic arc physical vapor deposition, Surf. Coat. Technol. 322 (2017) 211–217, https://doi.org/10.1016/j.surfcoat.2017.05.050.
[7] S. Mändl, D. Manova, Formation of hard coatings using plasma based ion implantation & deposition, in: Ronghua Wei (Ed.), Plasma Surface Engineering Research and Its Practical Applications, Research Signpost from Trivandrum, 2008, pp. 273–292.
[8] M.M.M. Bilek, D.R. McKenzie, R.N. Tarrant, S.H.M. Lim, D.G. McCulloch, Plasma-based ion implantation utilising a cathodic arc plasma, Surf. Coat. Technol. 156 (2002) 136–142, https://doi.org/10.1016/S0257-8972(02)00078-6.
[9] Golnaz Taghavi Pourian Azar, Dilan Er, Mustafa Ürgen, The role superimposing pulse bias voltage on DC bias on the macroparticle attachment and structure of TiAlN coatings produced with CA-PVD, Surf. Coat. Technol. 350 (2018) 1050–1057, https://doi.org/10.1016/j.surfcoat.2018.02.066.
[10] J.P. Quintana, J.M. Massone, A.B. Márquez, D.A. Colombo, Rolling contact fatigue behavior of TiN based coatings deposited on ADI by cathodic arc deposition and plasma based ion implantation and deposition, Thin Solid Films 671 (2019) 95–102, https://doi.org/10.1016/j.tsf.2018.12.014.
[11] B. Podgornik, J. Vizintin, Tribology of thin films and their use in the field of machine elements, Vacuum. 68 (2003) 39–47, https://doi.org/10.1016/S0042-207X(02)00282-8.
[12] W. Tillmann, E. Vogli, S. Momeni, Improvement of press dies used for the production of diamond composites by means of DUPLEX-PVD-coatings, Surf. Coat. Technol. 205 (2010) 1571–1577, https://doi.org/10.1016/j.surfcoat.2010.08.048.
[13] Y.Y. Chang, S. Amrutwar, Effect of plasma nitriding pretreatment on the mechanical properties of AlCrSiN-Coated tool steels, Materials. 12 (March 5) (2019) 795, https://doi.org/10.3390/ma12050795.
[14] L.S. Vaca, J.P. Quintana, M.A. Guitar, D. Vega, S.P. Brühl, A. Márquez, Influence of the pre-treatments and process temperature on the adhesion of TiN films deposited by PBII&D over nitrided austenitic stainless steel, Mater. Res. 22 (5) (2019) https://doi.org/10.1590/1980-5373-mr-2019-0282, São Carlos 2019 Epub Oct 28.
[15] K. Holmberg, A. Matthews, Coatings tribology. Properties, mechanisms, techniques and applications in surface engineering, In: second edition, in: B.J. Briscoe (Ed.), Tribology and Interface Engineering Series, vol. 56, 2009, Chapter 3..
[16] Xinxin Ma, Guangze Tang, Mingren Sun, Ken Yukimura, Characteristic of TiN films deposited on a trench-shaped sample prepared by plasma-based ion implantation and deposition, Surf. Coat. Technol. 196 (2005) 100–103, https://doi.org/10.1016/j.surfcoat.2004.08.110.
[17] F.M. El-Hossary, N.Z. Negm, A.M. Abd El-Rahman, M. Hammad, C. Templier, Duplex treatment of AISI 304 austenitic stainless steel using rf nitriding and dc reactive magnetron sputtering of titanium, Surf. Coat. Technol. 202 (8) (2008) 1392–1400, https://doi.org/10.1016/j.surfcoat.2007.06.066.
[18] E. De las Heras, D.A. Egidi, P. Corengia, D. González-Santamaría, A. García-Luis, M. Brizuela, G.A. López, M. Flores Martinez, Duplex surface treatment of an AISI 316L stainless steel; microstructure and tribological behavior, Surf. Coat. Technol. 202 (2008) 2945–2954, https://doi.org/10.1016/j.surfcoat.2007.10.037.
[19] L. Escalada, J. Lutz, S.P. Brühl, M. Fazio, A. Márquez, S. Mändl, D. Manova, S.N. Simison, Microstructure and corrosion behavior of AISI 316L duplex treated by means of ion nitriding and plasma based ion implantation and deposition, Surf. Coat. Technol. 223 (2013) 41–46, https://doi.org/10.1016/j.surfcoat.2013.02.025.
[20] A.K. Zak, W.A. Majid, M.E. Abrishami, R. Yousefi, X-ray analysis of ZnO nanoparticles by Williamson–Hall and size–strain plot methods, Solid State Sci. 13 (1) (2011) 251–256, https://doi.org/10.1016/j.solidstatesciences.2010.11.024.
[21] C. Godoy, R.D. Mancosu, R.R. Machado, P.J. Modenesi, J.C. Avelar-Batista, Which hardness (nano or macrohardness) should be evaluated in cavitation?, Tribol. Int. 42 (2009) 1021–1028, https://doi.org/10.1016/j.triboint.2008.09.007.
[22] S. Momeni, W. Tillman, M. Phol, Composite cavitation resistance PVD coatings based on NiTi thin films, Mater. Des. 110 (2016) 830–838, https://doi.org/10.1016/j.matdes.2016.08.054.
[23] A. Leyland, A. Matthews, On the significance of the H/E ratio in wear control: a nanocomposite coating approach to optimised tribological behavior, Wear. 246 (2000) 1–11, https://doi.org/10.1016/S0043-1648(00)00488-9.
[24] Standard Test Method for Adhesion Strength and Mechanical Failure Modes of Ceramic Coatings by Quantitative Single Point Scratch Testing, 2010C1624–05, Reapproved.
[25] VDI Standard, V.D.I. 3198 Coating (CVD -PVD) of Cool Forging Tools, 1992.
[26] Standard Test Method for Wear Testing With a Pin-on-Disk Apparatus G99 – 95a, 2000, reapproved.
[27] Standard Practice for Operating Salt Spray (Fog) B117 – 03, 2020.
[28] I. Zhirkov, A. Petruhins, J. Rosén, Effect of cathode composition and nitrogen pressure on macroparticle generation and type of arc discharge in a DC arc source with Ti–Al compound cathodes, Surf. Coat. Technol. 281 (2015) 20–26, https://doi.org/10.1016/j.surfcoat.2015.09.030.
[29] A. Anders, A structure zone diagram including plasma-based deposition and ion etching, Thin Solid Films 518 (15) (2010) 4087–4090, https://doi.org/10.1016/j.tsf.2009.10.145.
[30] D. Manova, J.W. Gerlach, S. Mändl, Thin film deposition using energetic ions, Materials 3 (8) (2010) 4109–4141, https://doi.org/10.3390/ma3084109.
[31] T.Y. Tsui, G.M. Pharr, W.C. Oliver, C.S. Bhatia, R.L. White, S. Anders, A. Anders, I.G. Brown, Nanoindentation and nanoscratching of hard carbon coatings for magnetic discs, Mrs Proc. (1995) 383–447, https://doi.org/10.1557/PROC-383-447.
[32] X. Zhang, S. Zhang, B.D. Beake, Toughness evaluation of thin hard coatings and films, in: S. Zhang (Ed.), Thin Films and Coatings: Toughening and Toughness Characterization, CRC Press, 2015, pp. 48–121.
[33] J. Musil, M. Jirout, Toughness of hard nanostructured ceramic thin films, Surf. Coat. Technol. 201 (9-11) (2007) 5148–5152, https://doi.org/10.1016/j.surfcoat.2006.07.020.
[34] U. Welzel, J. Ligot, P. Lamparter, A.C. Vermeulen, E.J. Mittemeijer, Stress analysis of polycrystalline thin films and surface regions by X-ray diffraction, J. Appl. Cryst 38 (2005) 1–29, https://doi.org/10.1107/S0021889804029516.
[35] G. Ma, L. Wang, H. Gao, J. Zhang, T. Reddyhoff, The friction coefficient evolution of a TiN coated contact during sliding wear, Appl. Surf. Sci. 345 (2015) 109–115, https://doi.org/10.1016/j.apsusc.2015.03.156.
[36] G.M. Uddin, A.A. Khan, M. Ghufran, Z.U.R. Tahir, M. Asim, M. Sagheer, M. Jawad, J. Ahmad, M. Irfan, B. Waseem, Experimental study of tribological and mechanical properties of TiN coating on AISI 52100 bearing steel, Adv. Mech. Eng. 10 (9) (2018), 1687814018802882. https://doi.org/10.1177%2F1687814018802882.
[37] J. Musil, Advanced hard coatings with enhanced toughness and resistance to cracking, in: S. Zhang (Ed.), Thin Films and Coatings: Toughening and Toughness Characterization, CRC Press, 2015, pp. 377–464.
[38] K. Holmberg, A. Matthewst, H. Ronkainen, Coatings tribology-contact mechanisms and surface design, Tribol. Int. (1998) https://doi.org/10.1016/S0301-679X(98)00013-9, Chapter 3..
[39] S. Achanta, T. Liskiewicz, D. Drees, J.-P. Celis, Friction mechanisms at the micro-scale, Tribol. Int. 42 (2009) 1792–1799, https://doi.org/10.1016/j.triboint.2009.04.018.
[40] J.M. Albella, Láminas Delgadas Y Recubrimientos. Preparación, Propiedades Y Aplicaciones, Consejo Superior de Investigaciones Científicas, Madrid, 2003, Chapter 20..
[41] Z. Yan, D. Jiang, X. Gao, M. Hu, D. Wang, Y. Fu, J. Sun, D. Feng, L. Weng, Friction and wear behavior of TiN films against ceramic and steel balls, Tribol. Int. 124 (2018) 61–69, https://doi.org/10.1016/j.triboint.2018.03.031.
[42] B.D. Beake, V.M. Vishnyakov, J.S. Colligon, Nano-impact testing of TiFeN and TiFeMoN films for dynamic toughness evaluation, J. Phys. D Appl. Phys. 44 (8) (2011), 085301 https://iopscience.iop.org/article/10.1088/0022-3727/44/8/085301.
[43] M.A. Domínguez-Crespo, A.M. Torres-Huerta, E. Rodríguez, A. González-Hernández, S.B. Brachetti-Sibaja, H.J. Dorantes-Rosales, A.B. López-Oyama, Effect of deposition parameters on structural, mechanical and electrochemical properties in Ti/TiN thin films on AISI 318L substrates produced by r.f. Magnetron sputtering, J. Alloys. Compd. 746 (2018) 688–698, https://doi.org/10.1016/j.jallcom.2018.02.319.
[44] K. Shukla, R. Rane, J. Alphonsa, P. Maity, S. Mukherjee, Structural, mechanical and corrosion resistance properties of Ti/TiN bilayers deposited by magnetron sputtering on AISI 316L, Surf. Coat. Technol. 324 (2017) 167–174, https://doi.org/10.1016/j.surfcoat.2017.05.075.
[45] Chenglong Liu, Guoqiang Lin, Dazhi Yang, Min Qi, In vitro behavior of multilayered Ti/TiN coating on biomedical AISI 316L stainless steel, Surf. Coat. Technol. 200 (2006) 4011–4016, https://doi.org/10.1016/j.surfcoat.2004.12.015.

[46] J. Vega, H. Scheerer, G. Andersohn, M. Oechsner, Experimental studies of the effect of Ti interlayers on the corrosion resistance of TiN PVD coatings by using electrochemical methods, Corros. Sci. 133 (2018) 240–250, https://doi.org/10.1016/j.corsci.2018.01.010.

[47] E.L. Dalibon, M. Moscatelli, S. Simison, L. Escalada, A. Cabo, C. Lasorsa, S.P. Brühl, Corrosion behaviour of a SiOxNy coated and nitrided PH stainless steel, Procedia Mater. Sci. 8 (2015) 29–38, https://doi.org/10.1016/j.mspro.2015.04.045.